Light-Induced Complete Reversal of Ferroelectric Polarization in Sliding Ferroelectrics

Qing Yang[1,4] and Sheng Meng[1,2,3,*]

[1]Beijing National Laboratory for Condensed Matter Physics and Institute of Physics, Chinese Academy of Sciences, Beijing 100190, China

[2]School of Physical Sciences, University of Chinese Academy of Sciences, Beijing 100049, China

[3]Songshan Lake Materials Laboratory, Dongguan 523808, China

[4]College of Physics and Electronic Science, Hubei Key Laboratory of Photoelectric Materials and Devices, Hubei Normal University, Huangshi 435002, China

(Received 14 December 2023; accepted 23 August 2024; published 27 September 2024)

Previous experiments have provided evidence of sliding ferroelectricity and photoexcited interlayer shear displacement in two-dimensional materials, respectively. Herein, we find that a complete reversal of vertical ferroelectric polarization can be achieved within an astonishing 0.5 ps in *h*-BN bilayer by laser illumination. Comprehensive analysis suggests that ferroelectric polarization switching originates from laser-induced interlayer sliding triggered by selective excitation of multiple phonons. The interlayer electron excitation from the p_z orbitals of the upper layer N atoms to the p_z orbitals of the lower layer B atoms produces desirable and directional interlayer forces activating the in-plane optical TO-1 and LO-1 phonon modes. The atomic motions driven by the coupling of TO-1 and LO-1 modes are coherent with ferroelectric soft mode, thus modulating the dynamical potential energy surface and resulting in ultrafast ferroelectric polarization reversal. Our work provides a novel microscopic insight into ultrafast polarization switching in sliding ferroelectrics.

DOI: 10.1103/PhysRevLett.133.136902

Ultrafast laser-induced phase transitions in quantum materials have opened up exciting possibilities for various applications in areas such as nanoprocessing [1,2], optical memory [3,4], and device fabrication [5,6]. To this end, important breakthroughs over the past decade include photo-induced insulator-metal transitions [7,8], laser-controlled magnetization switching [9–12], and the uncovering of hidden phases [13–16]. A remarkable target is light-induced ferroelectric (FE) polarization switching [17–21]. The ability to switch FE polarization optically opens up new possibilities for the development of ultrafast nonvolatile ferroelectric memories [22,23], which have advantages in terms of speed, energy efficiency, and nonvolatility compared to traditional memory technologies, making them attractive for future high-performance computing and data storage applications.

The traditional methods of FE polarization switching rely on external electric fields and face severe limitations such as the need for circuitry access and slow switching time in the nanosecond range [24,25]. To overcome these challenges, researchers have explored optical control of FE polarization, aiming to achieve faster switching down to the picosecond timescale [26,27]. However, practical implementation of this approach has been proven challenging, as intense laser pulses have only resulted in a FE polarization decrease or partial transient reversal in the past [17,28,29]. The reasons for these limitations and the possibility of achieving complete FE polarization reversal in ferroelectrics remain unclear, demanding more efficient mechanisms for laser-induced FE polarization reversal.

The sliding ferroelectricity was first proposed in the most nonferroelectric honeycomb lattices (*h*-BN, MoS_2) [30,31], where certain stacking configurations of bilayers or multilayers can break the symmetry and give rise to the switchable vertical polarizations through in-plane translation [32]. The experimental evidence of sliding ferroelectricity has detected in bilayer WTe_2 [33], which have been demonstrated theoretically that FE switching is caused by interlayer sliding [34,35]. Over the next few years, such ferroelectricity have been experimentally observed in *h*-BN [36,37], WSe_2 [38,39], MoS_2 [40–43], WS_2 [44], and organic crystal [45]. Additionally, previous experimental studies demonstrated that light pulses could induce interlayer shear strain with a large amplitude in layered WTe_2 [46,47], which provides experimental evidence for the achievement of laser-induced interlayer sliding [48]. However, neither of these works explored the realm of ultrafast FE polarization reversal. It is highly desirable to explore the ultrafast FE polarization switching in sliding ferroelectrics.

Here, we propose a mechanism to enable efficient switching of FE polarization in sliding ferroelectrics. First-principles simulations of ultrafast quantum dynamics (Note S1 [49]) in a photoexcited *h*-BN bilayer reveal that

*Contact author: smeng@iphy.ac.cn

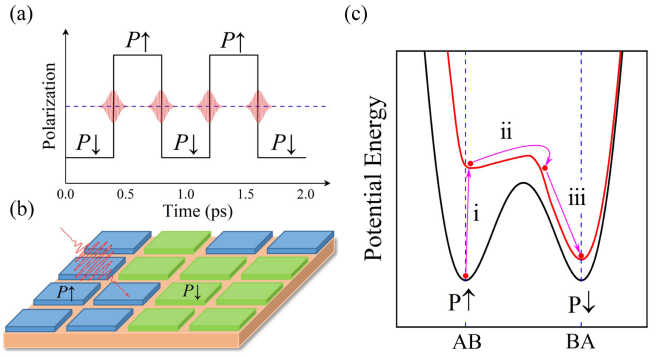

FIG. 1. (a) Diagram of ultrafast polarization switching. (b) Schematic diagram of ultrafast nonvolatile ferroelectric memories. (c) Diagram of laser-induced modification of potential energy surface (PSE). Black and red lines denote the PSEs in the ground and excited states, respectively.

FE polarization can be completely reversed within a mere 0.5 ps (corresponding to operation at 2.0 THz). A laser source could be utilized to switch FE polarization on the order of picoseconds, and reversibly switch it back [Fig. 1(a)]. This ultrafast FE switching through optical excitation holds a great potential in optoferroic devices, particularly in ultrafast nonvolatile ferroelectric memories. The blue and green blocks in Fig. 1(b) indicate the up- and down-polarized structures of *h*-BN bilayers, respectively, which can serve as bistable states equivalent to "0" and "1" in memory storage, with each block storing one bit of data. The ultrafast laser creates an efficient channel to efficiently alter the potential energy surface in a nonthermal way [Fig. 1(c)], enabling ultrafast FE switching.

The geometry structure of *h*-BN bilayer in the *AB*-stacking (*AB* state) is shown in Fig. 2(a), with a lattice parameter of $a = b = 2.50$ Å. The B atoms in the upper layer lie above the N atoms in the lower layer, while the N atoms in the upper layer are right over the hexagon center in the lower layer. Here, the close interlayer B-N distance and different electronegativity of the N and B atoms lead to the net charge transfer from the upper layer to the lower layer, resulting in a vertical FE polarization along the $+z$ direction. The FE polarization can be switched by interlayer sliding, moving the N atoms in the upper layer right over the B atoms in the lower layer, resulting in the *BA*-stacking (*BA* state) with a vertical FE polarization along the $-z$ direction [Fig. 2(b)].

The path and potential energy surface of FE polarization switching show that the multiple degenerate local minima in Fig. 2(c) correspond to the $AB-(BA-)$ stacking configurations, indicating that FE phase is the ground state. The distances from the *AB* state to the nearest and next nearest global minima *BA* state are $\sqrt{3}a/3$ and $2\sqrt{3}a/3$ Å, respectively. There are two paths to switch the *AB* state to the *BA* state through interlayer sliding, as denoted path I and path II in Fig. 2(d). For path I, the *AB*

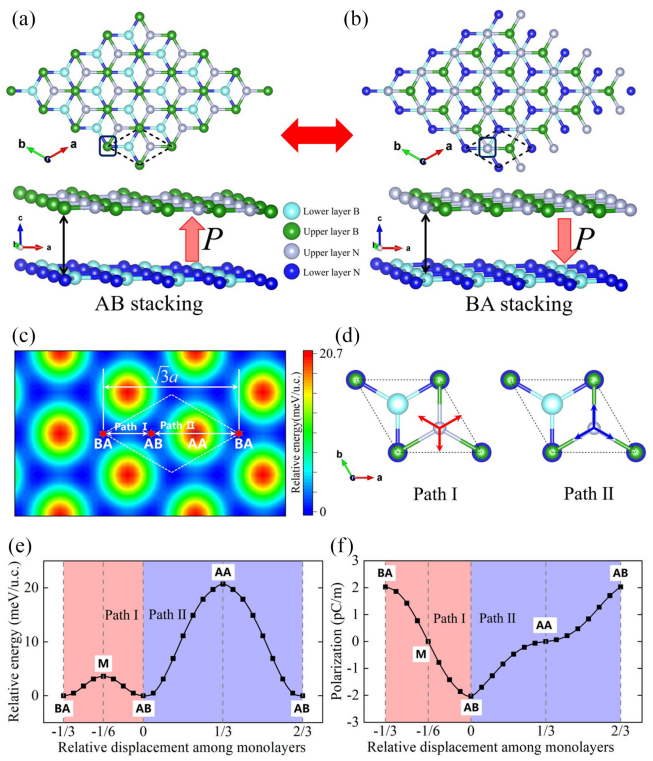

FIG. 2. (a),(b) Geometry structure of *AB* state and *BA* state in *h*-BN bilayer. (c) Energy landscape for *h*-BN bilayer as a function of the relative sliding among their constituent monolayers. (d) Two paths of FE polarization switching for *h*-BN bilayers. (e) Cut along a horizontal line on the landscape, the energy barrier for paths I and II are displaced. (f) The dependence of FE polarization from *AB* state to *BA* state on the sliding displacement along paths I and II.

state can be switched to the *BA* state under the interlayer translation operation along $t[1/3, 2/3, 0]$, $t[-2/3, -1/3, 0]$, or $t[1/3, -1/3, 0]$. For path II, the FE switching can be achieved through interlayer sliding along other three equivalent directions, defined as $t[-2/3, -4/3, 0]$, $t[4/3, 2/3, 0]$, or $t[-2/3, 2/3, 0]$. A one-dimensional cut of the energy landscape [Fig. 2(e)] is taken along the solid horizontal line depicted in Fig. 2(c). The energy barriers for FE switching along path I and path II are calculated to be 3.6 and 20.7 meV *per u.c.*, respectively, indicating that FE switching tends to occur along path I. The corresponding FE polarization is reversed in both path I and path II [Fig. 2(f)], and the two intermediate states are paraelectricity.

To study the electronic evolution and ionic dynamics in *h*-BN bilayer under the resonant excitation, we apply a Gaussian-type laser pulse linearly polarized along the *y* direction, perpendicular to FE polarization. In previous studies, Sharma *et al.* have used excitation fluences in the range of 20–80 mJ/cm^2 [61] in experimental measurements, the ultraviolet (UV) with 400 nm ($E_{\text{pump}} = 3.1$ eV) was used, which lies below the damage threshold for destroying the lattice structure of *h*-BN. We use a UV

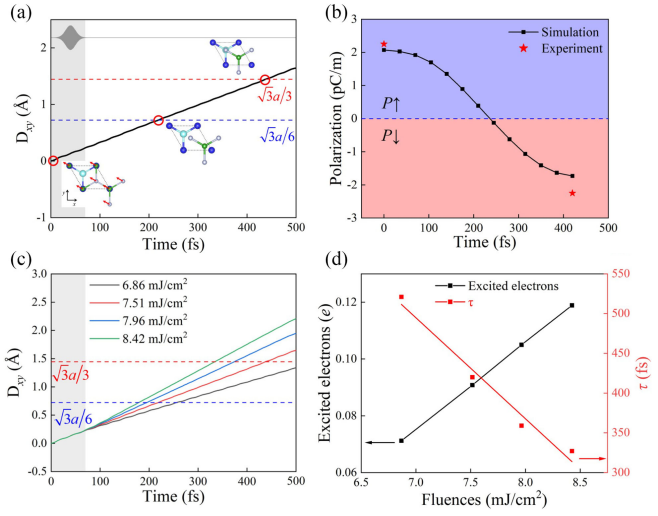

FIG. 3. (a) Time dependent relative interlayer sliding displacement along the lateral x-y plane. (b) Time dependent FE polarization of h-BN bilayer. The red stars are the experimentally measured values (Ref. [37]) without photoexcitation. (c) Time dependent relative interlayer sliding displacement along the lateral x-y plane with different laser fluences. (d) The time required for FE polarization switching (τ) and the number of excited electrons as a function of laser intensity.

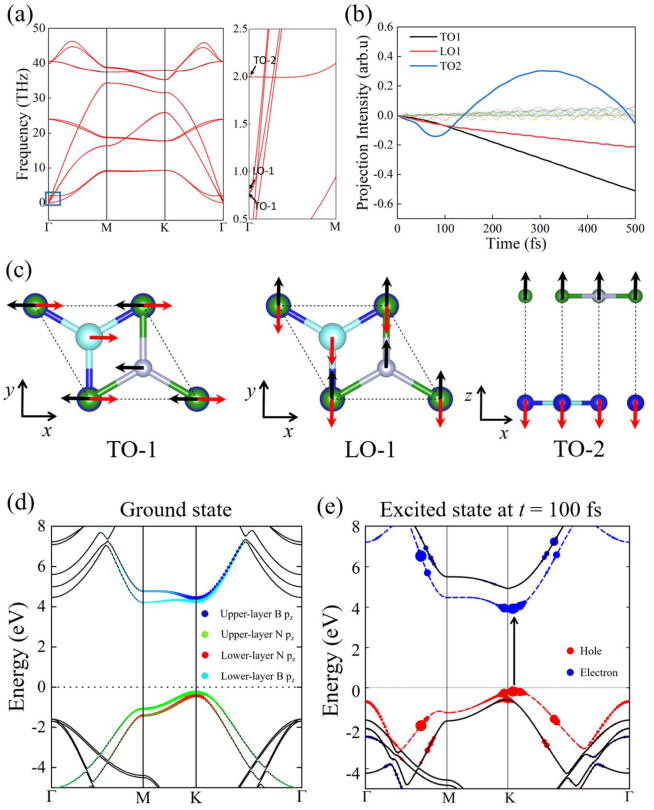

FIG. 4. (a) Phonon dispersion spectrum of h-BN bilayer in AB state. (b) Time evolution of all 12 Gamma-point projected phonon branches. (c) Vibrational modes of three excited phonons. (d) Orbital-resolved band structure of ground state. (e) Excited band structures at $t = 100$ fs.

laser pulse ($E = 4.14$ eV) with the fluence of 7.51 mJ/cm^2 [Fig. S2(a)], which is smaller than the experimental parameter, indicating that the laser intensity adopted here would not damage the h-BN bilayer. There are approximately 0.5% of valence electrons excited to the conduction bands after laser pulse ends at $t = 70$ fs [Fig. S2(b)].

The relative interlayer sliding directions under laser illumination are shown in Fig. 3(a), where the upper layer displacements (Note S2 [49]) along the lateral x-y plane relative to the lower layer. More importantly, the direction is consistent with path I for FE polarization switching, leading to the ultrafast FE polarization switching. Figure 3(a) depicts the upper layer displacement relative to the lower layer along the lateral x-y plane. Notably, with the laser fluence of 7.51 mJ/cm^2, D_{xy} increases rapidly to $\sqrt{3}a/6$ (~0.72 Å, the M state) at ~210 fs and then grows to $\sqrt{3}a/3$ (~1.44 Å, the BA state) after 420 fs. It is evident that a complete reversal of FE polarization can be achieved within a timescale of 420 fs. Subsequently, the interlayer sliding motion persists due to inertia. However, it is important to note that the potential energy surface associated with the continued sliding is significantly higher in magnitude compared to the barrier of FE polarization switching [Figs. 2(e) and S12]. Thus, the interlayer sliding displacement reaches its maximum extent at 540 fs and subsequently rebounds back to the BA stacking configuration (Fig. S3). It is clear that the linear shift does not perpetually continue but undergoes a reversal after reaching its maximum displacement.

In the above process of the ultrafast FE polarization switching, the first stage is the activation stage (0–210 fs): D_{xy} increases, but the distortion is not sufficient to destroy the geometric features. The second stage is FE polarization switching stage (210–420 fs), where the two layers are driven to opposite FE polarization along the lateral x-y plane. The third stage is stabilizing and forming the BA state (after 420 fs), where D_{xy} continues to move for some time due to inertia and eventually rebounds back to the stable state (BA state). We also calculate the time-dependent FE polarization as shown in Fig. 3(b). The simulated FE polarization of h-BN bilayer in the ground state is 2.07 pC/m, which is consistent with the experimental value [37] of 2.25 pC/m without laser illumination. It is evident that FE polarization is completely reversed at $t = 420$ fs, validating the feasibility of ultrafast complete FE polarization switching. In the ultrafast dynamic process, a quasiequilibrium state of BA stacking is reached at $t = 420$ fs, which closely resembles the ground state of BA stacking.

Phonons play a crucial role in laser-induced phase transitions in quantum materials, particularly in FE polarization switching. Figure 4(a) illustrates the phonon dispersion spectrum and all 12 eigenvectors of phonons at the Γ point for the AB state of h-BN bilayer. The absence

of imaginary frequencies over the entire Brillouin zone indicates the dynamical stability of the *AB* state. We also calculate the phonon dispersion spectrum for the *M* state as shown in Fig. S5(a), revealing pronounced soft optical modes at the Brillouin zone center Γ point (referred to as FE soft mode). From analysis of the phonon eigenvector and vibrational mode as shown in Fig. S5(b), the soft mode corresponds to the interlayer sliding motion in opposite directions, resulting in FE ground state due to the phonon softening.

We calculate the projected intensity of ion displacement on the 12 phonon eigenvectors in the equilibrium ground state. The projected intensity can be defined as $\sum \mathbf{d}_i \cdot \mathbf{v}_{ij}$, where $\mathbf{d}_i$ is the displacement vector of the ith atom from its ground state at $t = 0$ fs, and $\mathbf{v}_{ij}$ is the phonon eigenvector of the ith atom for the jth phonon branch. We obtained the projection intensity by projecting the real-time motion trajectory of the system onto the eigenvectors of the phonons. There are three optical phonons denoted as TO-1, LO-1, and TO-2 has been mainly excited by laser pulse [Fig. 4(b)]. More intriguingly, the optical phonons TO-1 and LO-1 are degenerated in vibrational frequency with the value 0.78 THz, which represent the system's lowest-energy optical phonon modes. Remarkably, vibrations of the two degenerate phonons TO-1 and LO-1 are in the lateral x-y plane with perpendicular vibration directions [Fig. 4(c)], which modes are consistent with that of FE soft mode. Thus, the coupling of the anharmonic displacements of TO-1 and LO-1 phonon modes is the key factor for triggering FE polarization switching in *h*-BN bilayer. The ratio of the anharmonic displacement of TO-1 mode to that of LO-1 mode is about $\sqrt{3}:1$, suggesting the excitation and coupling of the optical TO-1 and LO-1 modes are essential for triggering FE polarization switching.

The ultrafast laser field is exerted directly on the electron subsystem rather than the phonon subsystem. Figure 4(d) displays the orbital-resolved band structure of the *AB* stacking *h*-BN bilayer, revealing that the valence band maximum (VBM) and conduction band minimum (CBM) are at the high-symmetric *K* point, primarily contributed by the p_z orbitals. The VBM is contributed by the p_z orbitals of the upper layer N atoms while the CBM is contributed by the p_z orbitals of the lower layer B atoms. This vertical alignment of the p_z orbitals of the N and B atoms leads to a distortion in the orbital of the N atoms, resulting in the vertical FE polarization [36]. The band structure at $t =$ 100 fs after the laser illumination of *AB* stacking *h*-BN bilayer is shown in Fig. 4(e). The single-photon excitation process results in carriers being excited from the VBM to the CBM at the high-symmetric *K* point while the high-level excited carriers in other high-symmetry points may be caused by two-photon excitation process. In the *AB* state, the N atoms in the upper layer is not directly aligned with B atoms in the lower layer. Consequently, the photoexcited electrons primarily undergo a transformation from the p_z orbitals of the N atoms in the upper layer to the p_z orbitals of the B atoms in the lower layer. This process generates desirable and directional forces acting on the N and B atoms, leading to interlayer sliding, which is a crucial mechanism to FE polarization switching.

In laser-induced FE polarization switching, we examine the electron excitation and ion dynamics under linearly y-polarized laser pulse with different intensities. For atomic movements along the lateral x-y plane [Fig. 3(c)], with the increase of laser intensity, the relative interlayer displacements are accelerated, and the average velocity is almost linearly dependent on the laser intensity. This accelerated process of interlayer sliding results in a decrease in the switching time (τ) for FE polarization as the laser intensity increase [Fig. 3(d)]. The dependence of interlayer sliding on laser intensity stems from the fact that the number of photo-excited electrons is proportional to the applied laser intensity. With more excited electrons, the interatomic forces increase, simultaneously accelerating the interlayer sliding and reducing τ. Therefore, by varying the laser intensity, we can effectively control FE switching time, offering a practical means to tailor and optimize ultrafast FE polarization switching in sliding ferroelectrics. Indeed, the observed variations between simulations and experimental data can be influenced by the supercell size effects and the presence of impurities or defects within the material.

The mechanism of the ultrafast and complete reversal of FE polarization in *h*-BN bilayer can be extended to other bilayers, such as MoS_2 and $MoSe_2$ bilayers. Figures 5(a) and 5(b) provide an example of 3R-stacking MoS_2 bilayer, which has experimentally demonstrated to be ferroelectric with out-of-plane polarization [40]. Previous experiments have demonstrated that the interlayer shear displacement is induced by complex longer-timescale dynamics (with a duration of approximately 25 ps), as depicted in Fig. 5(c) under the terahertz laser pulse. The relative displacement (Δ) is defined as $\Delta = [(D_{xy} - D_0)/(D_1 - D_0)]$, where D_0 and D_1 are the interlayer sliding displacement along the x-y plane of the paraelectric and ferroelectric states, respectively. Their experiments have also revealed that this process is triggered by a volume change associated with the transformation, resulting in a complex longitudinally heterogeneous strain profile with strain waves propagating from the interfaces and complicated by substrate interactions [46]. This significant discovery provides experimental evidence for the achievement of laser-induced interlayer sliding. The lower layer slides through the intermediate state at $t = 320$ fs and then continues to slide along the x-y plane [Fig. 5(c)], indicating that FE polarization is reversed after $t = 320$ fs. The interlayer sliding is primarily attributed to the anharmonic motion of phonons driven by photoexcited carriers and electron-phonon coupling, which is completely different from the mechanism

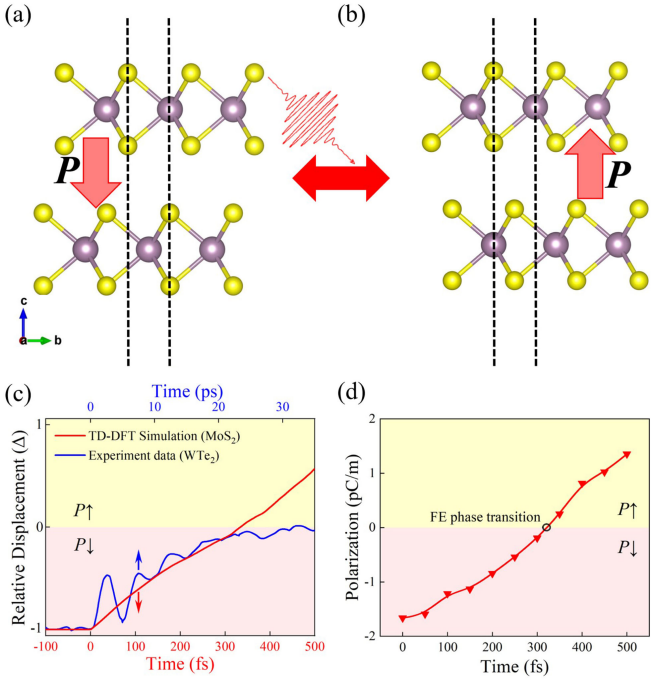

FIG. 5. (a),(b) Side view schematics of MoS_2 bilayer in down-polarized and up-polarized structures. (c) Laser-induced interlayer relative displacements (Δ) as a function of time along the lateral x-y plane of TD-DFT simulation in MoS_2 and experimental data in WTe_2 [46]. (d) Time-dependent FE polarization of MoS_2 bilayer.

of sliding observed in previous experiments [46]. Consequently, the timescale of interlayer sliding in our simulations is 0.5 ps, significantly faster than the experimental counterpart (25 ps). It is evident that FE polarization is zero at $t = 320$ fs and can be almost completely reversed at $t = 500$ fs [Fig. 5(d)], which confirms the feasibility of the laser-induced FE polarization reversal in 3R-stacking MoS_2 bilayer. Furthermore, we also confirm that the ultrafast FE switching is feasible in WTe_2 bilayer (Fig. S10), highlighting the potential for the ultrafast FE switching in sliding ferroelectrics.

In conclusion, we demonstrate that the ultrafast FE polarization switching in h-BN bilayer can be dissected into three substages: (i) The laser pulse raises the PES by excited electrons from the p_z orbitals of the upper layer N atoms to the p_z orbitals of the lower layer B atoms, inducing an asymmetrical charge order. (ii) These excited charge carriers transfer energy to the phonons, inducing anharmonic motion in the optical phonon modes through electron-phonon coupling. Atomic motions under these phonon modes induced opposite interlayer sliding. (iii) The photoexcited system relaxes to the ground state in conjunction with the dissipation of the photoexcited carriers, the system reaches the opposite FE state. Moreover, the mechanism of the ultrafast FE polarization reversal can be extended to other two-dimensional sliding ferroelectrics.

Acknowledgments—We acknowledge partial financial support from the National Natural Science Foundation of China (No. 12025407, No. 11934003, No. 11974400, No. 12147130 and No. 12404267), National Key Research and Development Program of China (No. 2021YFA1400201), and Chinese Academy of Sciences (No. YSBR-047 and No. XDB330301).

[1] S. Kawata, H.-B. Sun, T. Tanaka, and K. Takada, Nature (London) **412**, 697 (2001).
[2] K. Sugioka and Y. Cheng, Light Sci. Appl. **3**, e149 (2014).
[3] X.-B. Li, X. Q. Liu, X. Liu, D. Han, Z. Zhang, X. D. Han, H.-B. Sun, and S. B. Zhang, Phys. Rev. Lett. **107**, 015501 (2011).
[4] M. Wuttig and N. Yamada, Nat. Mater. **6**, 824 (2007).
[5] Y.-L. Sun, Q. Li, S.-M. Sun, J.-C. Huang, B.-Y. Zheng, Q.-D. Chen, Z.-Z. Shao, and H.-B. Sun, Nat. Commun. **6**, 8612 (2015).
[6] D. Yin, J. Feng, R. Ma, Y.-F. Liu, Y.-L. Zhang, X.-L. Zhang, Y.-G. Bi, Q.-D. Chen, and H.-B. Sun, Nat. Commun. **7**, 11573 (2016).
[7] M. Rini, R. A. Tobey, N. Dean, J. Itatani, Y. Tomioka, Y. Tokura, R. W. Schoenlein, and A. Cavalleri, Nature (London) **449**, 72 (2007).
[8] A. D. Caviglia, R. Scherwitzl, P. Popovich, W. Hu, H. Bromberger *et al.*, Phys. Rev. Lett. **108**, 136801 (2012).
[9] P. Zhang, T.-F. Chung, Q. Li, S. Wang, Q. Wang, W. L. B. Huey, S. Yang, J. E. Goldberger, J. Yao, and X. Zhang, Nat. Mater. **21**, 1373 (2022).
[10] A. S. Disa, M. Fechner, T. F. Nova, B. Liu, M. Först, D. Prabhakaran, P. G. Radaelli, and A. Cavalleri, Nat. Phys. **16**, 937 (2020).
[11] M. Först, A. D. Caviglia, R. Scherwitzl, R. Mankowsky, P. Zubko *et al.*, Nat. Mater. **14**, 883 (2015).
[12] S. Manz, M. Matsubara, T. Lottermoser, J. Büchi, A. Iyama, T. Kimura, D. Meier, and M. Fiebig, Nat. Photonics **10**, 653 (2016).
[13] L. Stojchevska, I. Vaskivskyi, T. Mertelj, P. Kusar, D. Svetin, S. Brazovskii, and D. Mihailovic, Science **344**, 177 (2014).
[14] J. Li, H. U. R. Strand, P. Werner, and M. Eckstein, Nat. Commun. **9**, 4581 (2018).
[15] T. F. Nova, A. S. Disa, M. Fechner, and A. Cavalleri, Science **364**, 1075 (2019).
[16] S. Prosandeev, J. Grollier, D. Talbayev, B. Dkhil, and L. Bellaiche, Phys. Rev. Lett. **126**, 027602 (2021).
[17] R. Mankowsky, A. von Hoegen, M. Forst, and A. Cavalleri, Phys. Rev. Lett. **118**, 197601 (2017).
[18] P. Chen, C. Paillard, H. J. Zhao, J. Iniguez, and L. Bellaiche, Nat. Commun. **13**, 2566 (2022).
[19] D. Shin, S. Latini, C. Schäfer, S. A. Sato, E. Baldini, U. De Giovannini, H. Hübener, and A. Rubio, Phys. Rev. Lett. **129**, 167401 (2022).
[20] J. Guo, W. Chen, H. Chen, Y. Zhao, F. Dong, W. Liu, and Y. Zhang, Adv. Opt. Mater. **9**, 2002146 (2021).
[21] M. Henstridge, M. Först, E. Rowe, M. Fechner, and A. Cavalleri, Nat. Phys. **18**, 457 (2022).
[22] R. Guo, L. You, Y. Zhou, Z. Shiuh Lim, X. Zou, L. Chen, R. Ramesh, and J. Wang, Nat. Commun. **4**, 1990 (2013).

[23] J. F. Scott and C. A. Paz de Araujo, Science **246**, 1400 (1989).
[24] J. Li, B. Nagaraj, H. Liang, W. Cao, C. H. Lee, and R. Ramesh, Appl. Phys. Lett. **84**, 1174 (2004).
[25] K. Fujimoto and Y. Cho, Jpn. J. Appl. Phys. **43**, 2818 (2004).
[26] T. Li, A. Lipatov, H. Lu, H. Lee, J. W. Lee, E. Torun, L. Wirtz, C. B. Eom, J. Iniguez, A. Sinitskii, and A. Gruverman, Nat. Commun. **9**, 3344 (2018).
[27] M.-M. Yang and M. Alexe, Adv. Mater. **30**, 1704908 (2018).
[28] A. Subedi, Phys. Rev. B **92**, 214303 (2015).
[29] V. Bilyk, E. Mishina, N. Sherstyuk, A. Bush, A. Ovchinnikov, and M. Agranat, Phys. Status Solidi (RRL) **15**, 2000460 (2021).
[30] L. Li and M. Wu, ACS Nano **11**, 6382 (2017).
[31] W. Jiang *et al.*, Phys. Rev. B **106**, 054104 (2022).
[32] L. Yang, S. Ding, J. Gao, and M. Wu, Phys. Rev. Lett. **131**, 096801 (2023).
[33] Z. Fei, W. Zhao, T. A. Palomaki, B. Sun, M. K. Miller, Z. Zhao, J. Yan, X. Xu, and D. H. Cobden, Nature (London) **560**, 336 (2018).
[34] Q. Yang, M. Wu, and J. Li, J. Phys. Chem. Lett. **9**, 7160 (2018).
[35] X. Liu, Y. Yang, T. Hu, G. Zhao, C. Chen, and W. Ren, Nanoscale **11**, 18575 (2019).
[36] K. Yasuda, X. Wang, K. Watanabe, T. Taniguchi, and P. Jarillo-Herrero, Science **372**, 1458 (2021).
[37] M. V. Stern, Y. Waschitz, W. Cao, I. Nevo, K. Watanabe, T. Taniguchi, E. Sela, M. Urbakh, O. Hod, and M. B. Shalom, Science **372**, 1462 (2021).
[38] X. Wang, K. Yasuda, Y. Zhang, S. Liu, K. Watanabe, T. Taniguchi, J. Hone, L. Fu, and P. Jarillo-Herrero, Nat. Nanotechnol. **17**, 367 (2022).
[39] S. Deb, W. Cao, N. Raab, K. Watanabe, T. Taniguchi, M. Goldstein, L. Kronik, M. Urbakh, O. Hod, and M. Ben Shalom, Nature (London) **612**, 465 (2022).
[40] A. Weston, E. G. Castanon, V. Enaldiev, F. Ferreira, S. Bhattacharjee *et al.*, Nat. Nanotechnol. **17**, 390 (2022).
[41] J. Liang, D. Yang, J. Wu, J. I. Dadap, K. Watanabe, T. Taniguchi, and Z. Ye, Phys. Rev. X **12**, 041005 (2022).
[42] D. Yang, J. Wu, B. T. Zhou, J. Liang, T. Ideue, T. Siu, K. M. Awan, K. Watanabe, T. Taniguchi, Y. Iwasa, M. Franz, and Z. Ye, Nat. Photonics **16**, 469 (2022).
[43] J. Wu, D. Yang, J. Liang, M. Werner, E. Ostroumov, Y. Xiao, K. Watanabe, T. Taniguchi, J. I. Dadap, D. Jones, and Z. Ye, Sci. Adv. **8**, eade3759 (2022).
[44] Y. Sun, S. Xu, Z. Xu, J. Tian, M. Bai, Z. Qi, Y. Niu, H. H. Aung, X. Xiong, J. Han, C. Lu, J. Yin, S. Wang, Q. Chen, R. Tenne, A. Zak, and Y. Guo, Nat. Commun. **13**, 5391 (2022).
[45] L.-P. Miao, N. Ding, N. Wang, C. Shi, H.-Y. Ye, L. Li, Y.-F. Yao, S. Dong, and Y. Zhang, Nat. Mater. **21**, 1158 (2022).
[46] E. J. Sie, C. M. Nyby, C. D. Pemmaraju, S. J. Park, X. Shen *et al.*, Nature (London) **565**, 61 (2019).
[47] S. Ji, O. Grånäs, and J. Weissenrieder, ACS Nano **15**, 8826 (2021).
[48] Q. Yang, C. Song, and S. Meng, J. Phys. Condens. Matter **34**, 424003 (2022).
[49] See Supplemental Material at http://link.aps.org/supplemental/10.1103/PhysRevLett.133.136902, with Refs. [50–60], for details about the theoretical methods and other discussion.
[50] G. Kresse and J. Furthmüller, Phys. Rev. B **54**, 11169 (1996).
[51] J. P. Perdew, K. Burke, and M. Ernzerhof, Phys. Rev. Lett. **77**, 3865 (1996).
[52] P. E. Blöchl, Phys. Rev. B **50**, 17953 (1994).
[53] S. Grimme, J. Antony, S. Ehrlich, and H. Krieg, J. Chem. Phys. **132**, 154104 (2010).
[54] S. Grimme, S. Ehrlich, and L. Goerigk, J. Comput. Chem. **32**, 1456 (2011).
[55] R. D. King-Smith and D. Vanderbilt, Phys. Rev. B **47**, 1651 (1993).
[56] G. Henkelman, B. P. Uberuaga, and H. Jónsson, J. Chem. Phys. **113**, 9901 (2000).
[57] S. Meng and E. Kaxiras, J. Chem. Phys. **129**, 054110 (2008).
[58] W. Ma, J. Zhang, L. Yan, Y. Jiao, Y. Gao, and S. Meng, Comput. Mater. Sci. **112**, 478 (2016).
[59] C. Lian, M. Guan, S. Hu, J. Zhang, and S. Meng, Adv. Theory Simul. **1**, 1800055 (2018).
[60] R. P. Feynman, Phys. Rev. **56**, 340 (1939).
[61] S. Sharma, S. Liu, J. H. Edgar, and I. Chatzakis, ACS Photonics **10**, 3586 (2023).